J Paleolimnol (2012) 48:175–192
DOI 10.1007/s10933-012-9619-0

ORIGINAL PAPER

Holocene climate change and landscape development from a low-Arctic tundra lake in the western Hudson Bay region of Manitoba, Canada

Philip Camill · Charles E. Umbanhowar Jr. · Christoph Geiss · William O. Hobbs · Mark B. Edlund · Avery Cook Shinneman · Jeffrey A. Dorale · Jason Lynch

Received: 30 August 2011 / Accepted: 9 April 2012 / Published online: 16 May 2012

Abstract The low-Arctic region of western Hudson Bay in interior Canada is one of the most poorly described areas of North America in terms of Holocene climate history. Here, we present new data from a well-dated lake sediment core from northern Manitoba, Canada. We assemble one of the richest multi-proxy datasets to date for a low-Arctic lake and characterize terrestrial and lake processes and exchanges between them. These proxies include fossil pollen and diatom assemblages, charcoal, magnetic properties (susceptibility and remanance), mineral grain size, bulk density, organic-matter content, elemental geochemistry, sediment cation (K^+, Mg^{2+}, Ca^{2+}, Fe^{2+}/Fe^{3+}) and macronutrient (P, N, C) contents, biogenic-silica content, basal peat dates (wetland initiation), and stable isotopes ($\delta^{13}C$, $\delta^{15}N$). The sediment proxies record both broad- and fine-scale (millennial and sub-millennial) climate change. We find indirect evidence for a cool and dry post-glacial period from 9,000 to 6,500 cal yr BP, a warm and moist mid-Holocene period from 6,500 to 2,500 cal yr BP, and a cool and moist late-Holocene period from 2,500 cal yr BP to present. High-resolution geochemical data suggests 300- to 500-year-long

This is one of 18 papers published in a special issue edited by Darrell Kaufman, and dedicated to reconstructing Holocene climate and environmental change from Arctic lake sediments.

Electronic supplementary material The online version of this article (doi:10.1007/s10933-012-9619-0) contains supplementary material, which is available to authorized users.

P. Camill (✉)
Environmental Studies Program and Department of Earth and Oceanographic Science, Bowdoin College, Brunswick, ME 04011, USA
e-mail: pcamill@bowdoin.edu

C. E. Umbanhowar Jr.
Department of Biology, St. Olaf College, Northfield, MN 55057, USA

C. Geiss
Department of Physics and Environmental Sciences Program, Trinity College, Hartford, CT 06106, USA

W. O. Hobbs · M. B. Edlund
St. Croix Watershed Research Station, Science Museum of Minnesota, Marine on St. Croix, MN 55047, USA

A. C. Shinneman
Department of Biology, University of Washington, Seattle, WA 98195, USA

J. A. Dorale
Department of Geoscience, University of Iowa, Iowa City, IA 52242, USA

J. Lynch
Department of Biology, North Central College, Naperville, IL 60540, USA

dry periods at ~6,500–6,100, 5,300–5,000, 3,300–2,800, and 400–0 cal yr BP. These results suggest that terrestrial and aquatic ecosystem dynamics in the western Hudson Bay region are sensitive to past climate change and are likely to respond to future changes in temperature and precipitation.

Keywords Arctic · Lake · Paleoclimate · Hudson Bay · Holocene · Proxy · Peat · Pollen · Diatom · Fire · XRF · Geochemistry

Introduction

The Holocene climate history of the western Hudson Bay region in interior Canada is poorly known. Although tree-ring studies have documented climate variations since the Little Ice Age (LIA) (Scott et al. 1988; Tardif et al. 2008), and modern observations are now showing rapid sea-ice loss and warming (Tivy et al. 2011), there is little information on long-term climate change and associated changes in ecological systems (Tillman et al. 2010). To our knowledge, no high-resolution, multi-proxy lake records with well-established chronologies exist for this region. Consequently, the timing and magnitude of earlier Holocene climate variations, including the Holocene thermal maximum (HTM), Neoglacial cooling (NGC), and Medieval climate anomaly (MCA) are poorly constrained (Kaufman et al. 2004; Viau and Gajewski 2009).

Developing a better understanding of climatic change and ecological responses in this region is important for several reasons. Central Canada marks a transition zone between earlier onset and termination of mid-Holocene warming in western North America, and later onset and termination in eastern North America (Kaufman et al. 2004). A data gap in this region hinders continental-scale synthesis efforts. Sea ice in Hudson Bay creates strong climatic linkages to terrestrial landscapes to the west (Rouse 1991). Periods of ice thaw may amplify terrestrial warming, whereas periods of ice formation reinforce cooling, possibly increasing the climate sensitivity of this region. Some of the largest changes in temperature and precipitation anywhere in the Arctic over the twentyfirst century are expected near Hudson Bay (IPCC 2007). Many of the sediment proxy records developed for the central and eastern regions of Canada (Joynt and Wolfe 2001; Michelutti et al. 2006, 2007; Fortin and Gajewski 2009; Paul et al. 2010; Peros et al. 2010) are from high-Arctic regions, which could differ substantially from low-Arctic sites that are influenced to a greater degree by terrestrial vegetation and peatlands. Finally, given the significant soil carbon density in the Hudson Bay Lowlands (Yu et al. 2011), warming in this region may increase carbon release, which could feed back significantly on climate.

Although lake ecosystems serve as important sentinels for climate change (Adrian et al. 2009; Leavitt et al. 2009; Schindler 2009), lake ecosystem processes and ontogeny are complicated by catchment-level factors that also influence biogeochemical processes (Anderson et al. 2008; Adrian et al. 2009; Kosten et al. 2009). Debate continues as to whether Arctic lakes are controlled more strongly by catchment factors (Anderson et al. 2008) or direct forcing by climate (Michelutti et al. 2007). Climate change may directly impact aquatic ecosystem processes, such as diatom productivity and species composition or pH (Wolfe 2002; Rühland et al. 2003; Fortin and Gajewski 2009; Paul et al. 2010), but it may also affect lakes indirectly through changes in the terrestrial ecosystem, such as climate-driven shifts in fire or vegetation and peatland expansion and their attendant export of DOC or N (Hu et al. 2001). Lakes may also respond to terrestrial changes unrelated to climate, such as local successional dynamics or lake/landscape ontogeny (Engstrom and Fritz 2006) or poor buffering capacity caused by base-cation-depleted parent materials (Michelutti et al. 2006). Understanding Arctic climatic responses using lake sediment records therefore requires a sufficient number of proxies sensitive to climate that are capable of distinguishing aquatic and terrestrial responses and their interactions.

We present new data from a well-dated lake sediment core from northern Manitoba, Canada documenting Holocene changes in both terrestrial and lake processes. We assemble a rich multi-proxy dataset in order to characterize terrestrial and lake processes and exchanges between them. These proxies include fossil pollen and diatom assemblages, charcoal, magnetic properties (magnetic susceptibility and remanence), mineral grain size, bulk density, organic-matter content, elemental geochemistry, sediment cation (K^+, Mg^{2+}, Ca^{2+}, Fe^{2+}/Fe^{3+}) and macronutrient content (P, N, C), biogenic silica (BSi) content, basal peat dates (wetland initiation), and stable isotopes ($\delta^{13}C$, $\delta^{15}N$). We examine the following

specific questions: (1) Do terrestrial and aquatic proxies at this site record the magnitude and timing of Holocene-and millennial-scale climatic changes, including the HTM, NGC, MCA, and LIA? (2) To what extent are proxies of aquatic processes versus terrestrial processes more useful for detecting climate change in this region?

Study region

Located approximately 140 km to the west of Hudson Bay, Unit Lake (unofficial name) lies along the modern woodland-tundra transition just south of the border between Manitoba and Nunavut (59°24′16″N, 97°29′34″W; Fig. 1a, b). Surficial geology is characterized by coarse glacial deposits bordered by proximal glaciofluvial sand and gravel (Matile and Keller 2006). The bedrock consists of Paleoproterozoic intrusive hybrid granite (Schledewitz and Lindal 2002). Unit Lake lies in a relatively high topographic position in a region defined by extensive lakes and lowland, peat-forming forests and wetlands (Fig. 1b, c). The lake is oriented along a N–S axis, and the bathymetry shows that the southern half of the lake consists of a deeper basin with a flat sediment surface (maximum depth 11.4 m), whereas the northern half of the basin rises to a shallower bench <2 m (Fig. 1c). Aquatic and watershed properties of Unit Lake are reported in Table 1.

Materials and methods

Sediment retrieval and dating

Non-overlapping sediment cores (total core length = 3.96 m) were retrieved from the deepest location in the lake basin during the summer of 2003. A clear polycarbonate piston corer (6.5-cm diameter) was used to retrieve the upper 1 m of flocculent material, and a modified Livingstone corer (4.8 cm diameter) was used to collect sediment at depth. Sediment from the polycarbonate tube was sectioned in the field at 1 cm intervals with the exception of the upper two sections (0–4 and 4–6 cm). To aid in the interpretation of landscape development, we also recovered five permafrost peat cores for basal radiocarbon dating using a modified Hoffer probe during the summers of 2008–2009. The lengths of the peat cores ranged from 37 to 131 cm. Cores were refrigerated (~4 °C) in the field until transported back to the laboratory, where they were maintained in cold storage (4 °C). Analyses were generally performed within 1 year, and geochemical proxies were conducted with freeze-dried sediment sampled within months of core retrieval.

Age control for the lake core was based on eight AMS ^{14}C dates, and surface sediments were dated using the ^{210}Pb method (constant rate of supply model, Appleby and Oldfield 1978) (Table 2). Basal peat dates were determined using AMS ^{14}C dating of terrestrial macrofossils (Table 2). We developed a probabilistic age-depth model for the lake sediments using CLAM v.1.2. (Blaauw 2010). Calibrated radiocarbon dates presented in Table 2 were calibrated with CALIB v.6.0 (Stuiver et al. 1999) to derive the median date of the probability density function. All dates are reported in calendar years BP (hereafter, BP). Our core sections were non-overlapping, and depths for drives 2–4 were based on field-measured distance to the water surface. Based on examination of AMS ^{14}C dates, organic-matter content, and magnetics, the depths for drive 1 were adjusted upwards, producing a short gap (~17 cm, ~313 year) between drives 1 and 2 that is reported in all figures.

Sediment properties

We used loss on ignition (LOI) to characterize the relative fractions of sediment organic matter, $CaCO_3$, and residual inorganic clastics. Samples of known volume (1 cm^3) and dry mass were combusted in a muffle furnace at 550 and 1,000 °C to determine the weight percent of organic and $CaCO_3$ fractions, respectively, and corrected for molecular weight differences between CO_2 and CO_3 (Dean 1974). Mean (median) sample resolution for LOI data was 80 (81) years.

We measured magnetic susceptibility (χ), isothermal remanent magnetization (IRM), and anhysteretic remanent magnetization (ARM) in P15 plastic cubes (volume = 5.3 cm^3) as proxies for ferrimagnetic mineral concentration and size following the methods of Geiss et al. (2003). χ and IRM characterize the concentration of ferrimagnetic minerals of all grain sizes, while ARM is strongly influenced by the presence of small single-domain (SD) and small

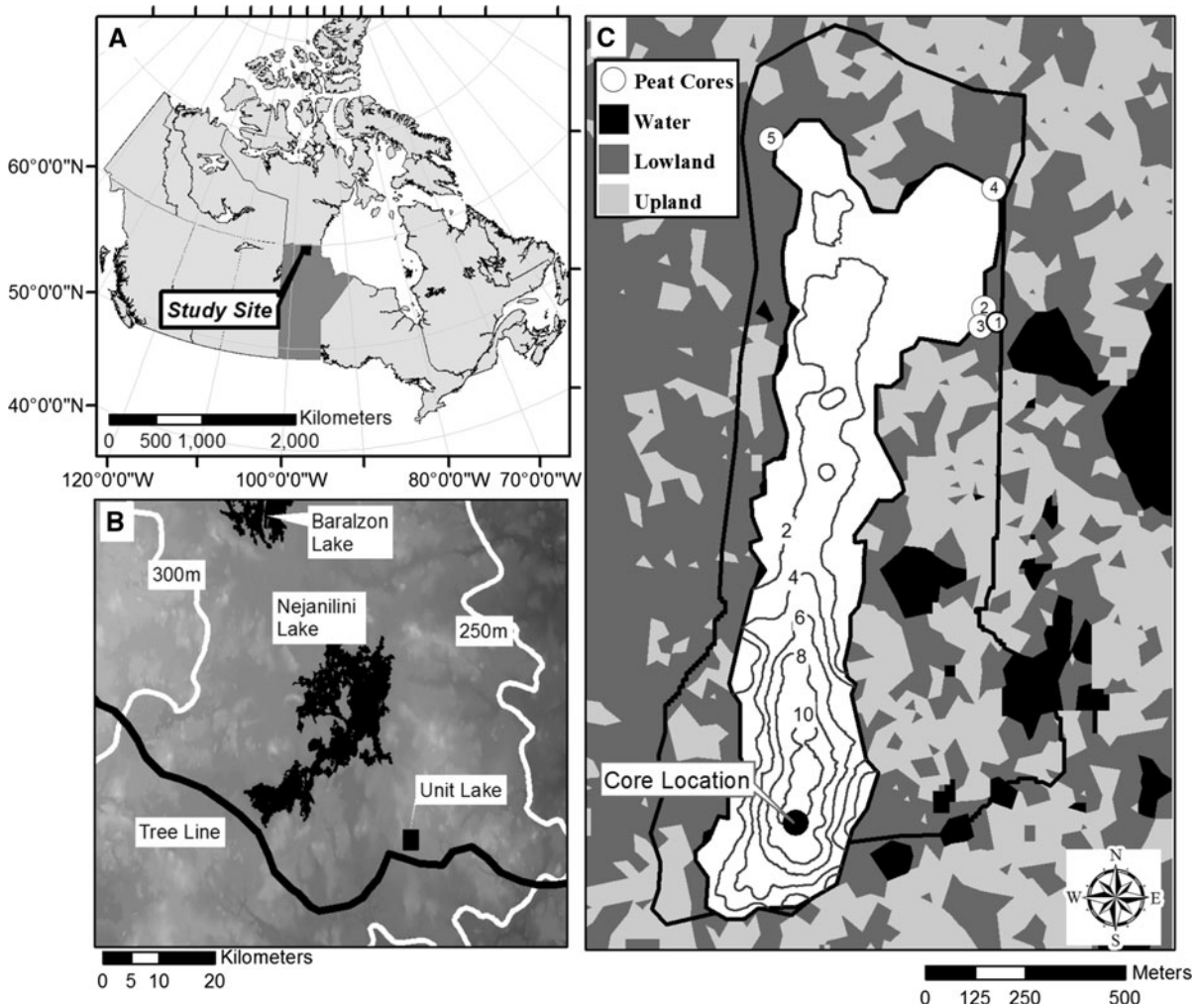

Fig. 1 **a** Location of study site along the border between Manitoba and Nunavut, Canada. **b** Landscape topography based on the digital elevation model for Manitoba (Canadian Digital Elevation Data, 1:50,000 downloaded from www.geobase.ca, 2005) and the location of Unit Lake relative to the modern-day woodland-tundra border. **c** The Unit Lake watershed boundary (*black line*), land cover classes, and lake bathymetry (contours = m) relative to the location of the lake sediment and peat sediment coring sites

pseudo-single-domain (PSD) ferrimagnetic particles between 0.01 and 1 μm. Changes in ARM/IRM reflect the relative importance of these fine grains versus larger multi-domain (MD) particles. All measurements were made at the Institute for Rock Magnetism at the University of Minnesota. Mean (median) sample resolution for magnetics data was 44 (44) years.

Grain size was determined using ~1.0–3.0 g samples (dry mass) digested for 30–60 min in 30 % H_2O_2 (or until reaction finished), followed by an additional 10 min in 11 M HNO_3 (Triplett 2002). BSi was removed using 1 M NaOH for 45 min, and samples were neutralized with 0.5 N HCl. The samples were rinsed into centrifuge tubes with deionized water and methanol, and centrifuged at 4,500 rpm for 15 min. Processed sediment was measured using a Horiba LA-920 particle analyzer at the University of Minnesota. Mean (median) sample resolution for the grain size analysis was 224 (192) years.

Cations (Ca^{2+}, Mg^{2+}, Fe^{2+}/Fe^{3+}, K^{+}) were extracted from ~0.10 g samples (dry mass) with a combination of 30 % H_2O_2 and 2.5 M HCl (Engstrom and Wright 1984). Cations were analyzed on a Horiba Jobin–Yvon Ultima 2 OES-ICP at St. Olaf College.

Concentration data for cations is reported as mg g^{-1}. Mean (median) sample resolution for the cation data was 148 (132) years.

Bulk elemental composition of sediment was measured at the University of Minnesota Duluth using the Large Lakes Observatory's ITRAX X-ray fluorescence (XRF) core scanner (Cox Analytical Instruments). The scanner was operated at 1 cm resolution on archival sections of Livingston drives and at 1–2 cm intervals on sediments from 0 to 20 cm tops of cores that had been previously sectioned in the field. Cores were scanned with 60 s scan times using a Mo X-ray source set to 30 kV and 15 mA. Mean (median) sample resolution for the XRF data was 26 (25) years. A small data gap between ~6,900 and 7,050 BP resulted from sediment consumption for dating and other analyses.

We measured the concentrations, stoichiometric ratios, and isotopic composition of macronutrient elements (C, N, P, Si) in the sediment cores. Total phosphorus (TP) was measured on freeze-dried sediments that were ground lightly with mortar and pestle, following the extraction procedures of Engstrom and Wright (1984). Extracted P was analyzed colorimetrically using a Lachat QC 8000 FIA system (method 10-115-01-1-B). We measured BSi as a proxy for plankton productivity. Following Conley and Schelske (1993), we extracted silica from 30 mg of freeze-dried sediment using a 1 % Na_2CO_3 solution. Concentrations of BSi were determined colorimetrically on 3, 4, and 5 h digests (Conley 1998) using a Lachat QC 8000 FIA system (method 10-114-27-1-A) and slope-corrected or averaged across the three measurements as recommended by Conley (1998). Mean (median) sample resolution for the TP and BSi data was 88 (87) years. Total carbon (TC), total nitrogen (TN), $\delta^{13}C$, and $\delta^{15}N$ were measured on the bulk organic fraction. Samples were acidified in 1 M HCl, rinsed three times with deionized water, freeze dried then measured using a Costech CHNS analyzer. Analyses were done at the University of Iowa, Paul H. Nelson Stable Isotope Laboratory, and the UC Davis Stable Isotope Laboratory. Mean (median) sample resolution for the C, N, and isotope data was 162 (160) years. We report C:N, BSi:TP, and TN:TP as molar ratios. Concentration data for TP and BSi are given as mg g^{-1} and as percents for C and TN.

Table 1 Limnological and watershed properties of Unit Lake

Property	Value
Surface water[a]	
pH	5.74
Specific conductivity	16.76 µS cm^{-1}°C^{-1}
DOC	3.16 mg L^{-1}
Ca^{2+}	0.75 mg L^{-1}
Mg^{2+}	0.37 mg L^{-1}
K^{+}	0.25 mg L^{-1}
$Fe^{2+/3+}$	0.014 mg L^{-1}
TP	11.44 µg L^{-1}
Catchment area	148.4 ha
Lake area	64.4 ha
Land cover types	
Peat-forming vegetation[b]	40 %
Dry tundra	32 %
Woodland	9 %
Moist/wet tundra	8 %
Bare rock or till	6 %
Ponds	4 %

[a] Water properties are the mean values measured in July 2008/2009

[b] Peat moss and sedge peat with scattered to >50 % cover of *P. mariana*

Pollen and diatom analysis

Pollen analysis was conducted on 0.3–1.0 cm^3 samples using standard palynological methods (Fægri et al. 1989). An average of 409 pollen grains were counted per sample (min = 202, max = 515) in addition to an exogenous spike (*Eucalyptus globula*). Mean (median) sample resolution for pollen data was 92 (88) years. To separate *Picea mariana* from *P. glauca*, we examined between 80 and 100 *Picea* pollen grains per sample and differentiated them based on saccus shape, attachment reticulum, and saccus area/corpus area (Hansen and Engstrom 1985). The percentage of each species obtained was applied to the total number of *Picea* grains counted to estimate the proportion of *P. glauca* and *P. mariana*. McAndrews et al. (1973) was used for pollen and spore identification.

Samples for diatom analysis were collected from the split core at selected intervals and freeze dried. Sediments were processed using standard techniques for the oxidation of both carbonate minerals (10 % HCl)

Table 2 Radiocarbon and ^{210}Pb ages, Unit Lake

Laboratory sample[a]	Sediment depth (cm)[b]	^{14}C year BP	Calibrated year BP[d]	Material dated
(A) Lake sediment AMS ^{14}C				
CAMS-110421	28	1,070 ± 40	981 ± 59	Charcoal
CAMS-107023	98	2,120 ± 50	2,100 ± 74	Charcoal + woody scale
CAMS-107022	106	2,350 ± 60	2,402 ± 167	Charcoal
CAMS-107024	131	2,650 ± 45	2,770 ± 49	Charcoal
CAMS-107025	157	3,180 ± 45	3,406 ± 38	Charcoal
CAMS-109289	217.5	3,795 ± 40	4,182 ± 73	Woody twig
CAMS-110422	271	4,815 ± 40	5,524 ± 58	Charcoal
CAMS-109288	362	7,050 ± 140	7,873 ± 133	Woody scale
Laboratory sample[a]	Sediment depth (cm)[c]	^{14}C year BP	Calibrated year BP[d]	Material dated
(B) Basal peat AMS ^{14}C				
CAMS-143312	37	2,090 ± 50	2,064 ± 63	*Picea* needles
CAMS-143313	56	920 ± 70	836 ± 70	Bark, *Picea* needles
CAMS-143314	75	3,490 ± 35	3,766 ± 56	Bark, woody twig, needle
CAMS-143315	131	6,195 ± 35	7,087 ± 72	Bark woody twig
CAMS-143316	35	2,460 ± 50	2,539 ± 167	Bark, woody stem

Sediment depth (cm)[c]	Unsupported activity (pCi g^{-1})	Error (±1σ)	Age (yr)	Error (±1σ)	Date (AD)	Date (BP)
(C) Lake sediment ^{210}Pb dating						
0						−53
4	25.64	0.83	23.6	0.98	1,980	−30
6	20.00	0.69	55.9	0.85	1,948	2
7	13.00	0.25	71.0	1.03	1,933	17
8	8.50	0.35	87.0	1.20	1,917	33
9	6.52	0.27	121.8	1.55	1,882	68
10	2.49	0.12	147.4	2.51	1,856	94
11	0.98	0.07	178.0	5.29	1,826	124
12	0.39	0.06	200.7	9.29	1,803	147
13	0.018	0.06	232.3	17.40	1,771	179

[a] Center for Accelerator Mass Spectrometry, Lawrence Livermore National Laboratory, Livermore, California, USA

[b] Mid-point depth of interval

[c] Basal depth of interval

[d] Calibrated using CALIB v. 6.0. Age represents the median of the probability density function. Error represents one-half of the 1σ range

and organic matter (30 % H_2O_2). Samples were allowed to settle passively, the supernatant was aspirated, and the sample was rinsed three times with deionized water. Diluted slurries were permanently mounted for diatom enumeration using Naphrax®. Diatoms were enumerated under oil immersion (N.A. = 1.4) at a magnification of 1,000× using differential interference contrast optics. Three published floras were used for identification: Krammer and Lange-Bertalot (1986–1991), Camburn and Charles (2000), and Fallu et al. (2000). Photomicrographic documentation was conducted throughout the study under light microscopy. Mean (median) sample resolution for diatom data was 282 (273) years.

A diatom-inferred pH weighted-averaging transfer function was applied to the Unit Lake core using a 44-lake training set spanning a 18,000 km^2 region of northern Manitoba; modern pH values ranged from 4.39 to 6.98, with a mean and median of 5.76. Field pH measurements were adjusted upwards to account for

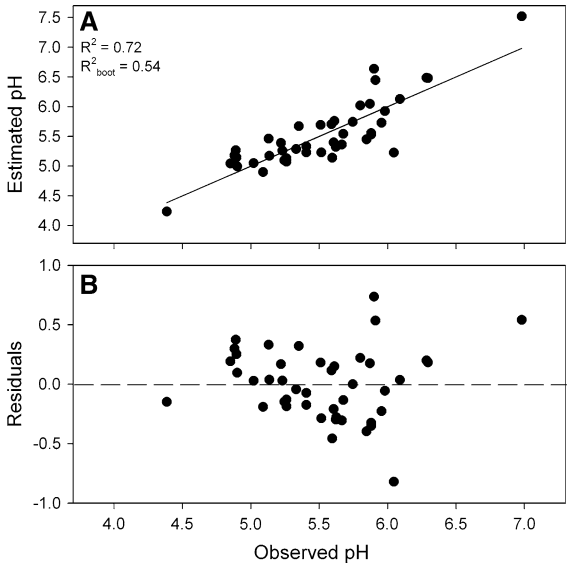

Fig. 2 **a** pH values inferred from the transfer function compared to observed pH in the calibration set, and **b** the residuals from the relationship

probe movement effects on pH, which have been reported previously (for example Hoenicke et al. 1991). Our lab tests indicated a mean pH depression of 0.65 (SD = 0.22, n = 12) associated with experimental stirring (120 rpm) of low conductivity (10–20 μS cm^{-1} $°C^{-1}$) solutions. The transfer function was developed and the predictive ability assessed using a weighted-averaging approach with bootstrap error estimation (Fig. 2). The strength of each model was assessed using the coefficient of determination ($R^2 = 0.72$) and the root mean square error (RMSE = 0.29). Because the same data were used to generate and evaluate the model, these assessments were not entirely independent, and the validation step of bootstrapping with 1,000 cycles was used to generate a bootstrapped coefficient of determination ($R^2_{boot} = 0.54$) and a root mean square error of prediction (RMSEP = 0.33), which more realistically portrays error estimates (Fritz et al. 1999). Transfer functions were developed using a weighted-averaging calculation with classic de-shrinking; both classic and inverse de-shrinking were evaluated and gave very similar R^2 and RMSEP values. De-shrinking corrects the overestimation of low values and underestimation of high values caused by averaging in both the regression and calibration steps of model development. Species abundances were not transformed or downweighted prior to running the model. All weighted-averaging calculations were made using the program C2 (Juggins 2003).

Charcoal analysis

We used macroscopic charcoal area as a proxy for fire severity and biomass burned (Clark et al. 1996; Camill et al. 2003). Sediment samples of 1 cm^3 were soaked in 10 % KOH for 48 h and sieved with a 180 μm nylon mesh screen. Charcoal fragments were identified at 20× magnification with a stereoscope, and the total charcoal areal concentration (mm^2 cm^{-3}) was measured using image analysis (Scion Image). Mean (median) sample resolution for fire data was 88 (87) years.

Statistical methods

Detrended correspondence analysis (DCA) was used to summarize the dominant gradient (i.e., DCA axis 1) of diatom compositional turnover (Hill and Gauch 1980). All diatom species were included in the analysis, detrending was by segments with down-weighting of rare taxa, and non-linear rescaling was applied. When plotted stratigraphically the DCA axis 1 scores shows the amount of turnover between samples over time in units of standard deviation (SD). A stratigraphically constrained cluster analysis was used to determine zones within the diatom and pollen stratigraphy using the approach of Grimm (1987) based on Bray-Curtis dissimilarity distances. Cluster analyses included diatom species with abundances >1 % and pooled pollen and spore abundances. The zones were based on a uniform total sum-of-squares height and statistical significance was tested against a random broken-stick model (Bennett 1996).

Results[1]

Sediment chronology

Based on the relationship between CLAM-derived calibrated ages and sediment depth, the total core length dated to 8,737 cal year BP (Fig. 3a). The

[1] All of the data from Unit Lake presented in this study are available on-line through the World Data Center for Paleoclimatology (http://www.ncdc.noaa.gov/paleo/pubs/jopl2012arctic/jopl2012arctic.html).

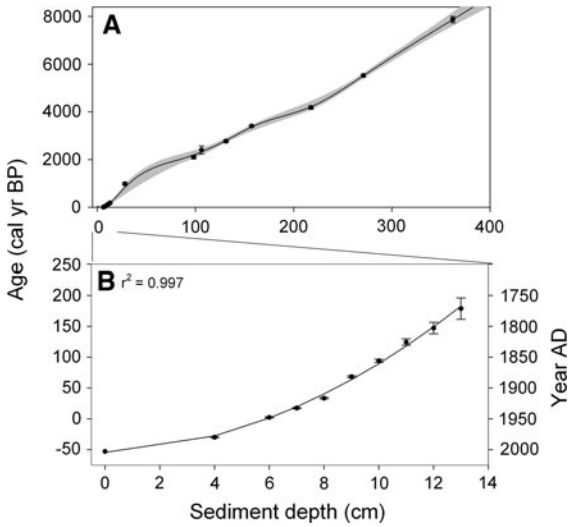

Fig. 3 Age-depth model for Unit Lake. **a** CLAM-derived model for the entire Holocene. Points represent calibrated ages from CALIB v.6.0 based on the median of the probability density function. Error represents one half of the 1σ range. **b** ^{210}Pb chronology based on data presented in Table 1. Error represents $\pm$1σ of the age

CLAM model was used to extrapolate the basal age at 3.96 cm, below the lowest AMS ^{14}C date located at 3.62 m (Table 2). Sedimentation appeared to be relatively constant throughout the Holocene (mean = 0.05 cm year^{-1}), although it was lowest (<0.04 cm year^{-1}) during the early Holocene from 8,737 to 4,600 BP, and highest (>0.07 cm year^{-1}) during the mid-to-late Holocene from 4,038 to 3,585 and 2,160–1,760 BP (excluding surface sediments). The ^{210}Pb dating indicated that the asymptote of unsupported activity was reached at 13 cm depth, corresponding to 179 BP (1771 AD) (Fig. 3b).

Mineral sediment properties

During the early Holocene (9,000–6,500 cal year BP), mineral inputs into Unit Lake were high (Fig. 4), reflecting erosion in a post-glacial tundra landscape. Relatively high Ti counts (a conservative marker of mineral weathering and erosion; Boës et al. 2011), high bulk density, and enriched base cations (especially K^+), in combination with fine grain size (little sand), suggest that this sediment comprises fine-grained, glacial mineral material that pre-dated significant organic accumulation in the lake (Kylander et al. 2011). Organic matter and $CaCO_3$ content are low (Fig. 4), likely indicating low aquatic productivity and little input of terrestrial organics at this time, although elevated sediment TC:TN ratios (see below) suggest a higher proportion of terrestrial material. Although we have not confirmed whether $CaCO_3$ is allochthonous or autochthonous using scanning electron microscopy, a lake pH <6.0 for most of the Holocene (see below) suggests that carbonate production was allochthonous. High values for IRM, combined with low ARM:IRM ratios, indicate an initial input of mostly coarse-grained (MD) ferrimagnetic minerals. IRM declined around 8,000 BP as organic matter rose, suggesting that ferrimagnetic iron oxide minerals began to dissolve under anoxic sediment conditions.

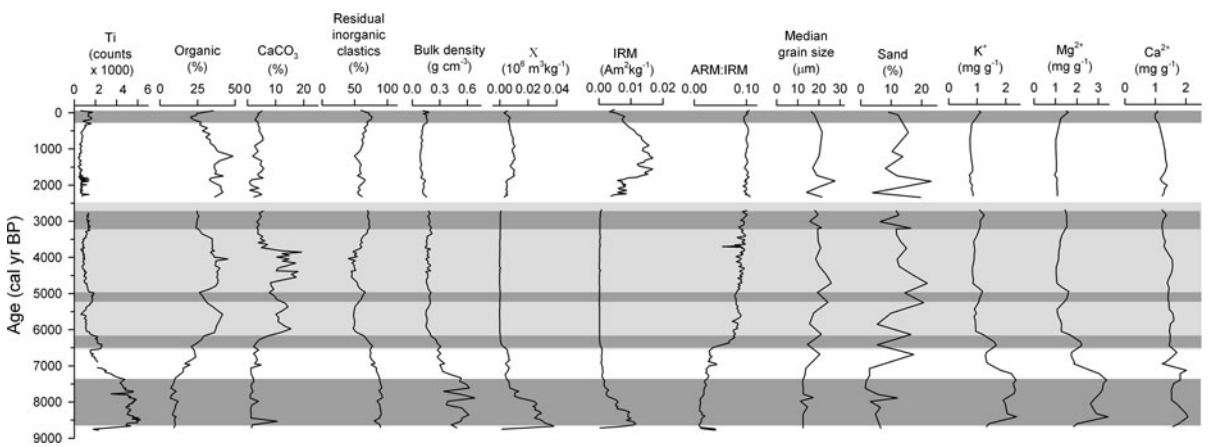

Fig. 4 Composition of sediment deposited in Unit Lake during the Holocene. *Light-gray shading* denotes the mid-Holocene (~6,500–2,500 BP). *Dark-gray shading* denotes periods of relatively high Ti input (detrital inputs of mineral materials)

The transition to the mid-Holocene was marked by substantial change in sediment composition (Fig. 4). By 6,000 BP, detrital mineral inputs had declined, and the organic-matter and $CaCO_3$ contents increased. Median grain size and the proportion of sand increased but were variable. The rise in ARM:IRM suggests the predominance of small SD and PSD (0.01–1 μm) ferrimagnetic particles, which are likely microbial (Moskowitz et al. 1988).

The late Holocene (~2,500 BP—present) was characterized by the lowest detrital mineral input of the Holocene (Fig. 4). After declining between 3,300 and 2,800 BP, organic-matter content rose between 2,500 and 500 BP. Carbonate content was consistently low throughout this period. Median grain size and the proportion of sand were variable but decreased toward the late Holocene. Higher concentrations of Fe are reflected in increased χ and IRM, but the magnetic component continued to be fine grained (high ARM:IRM).

In addition to these broad secular trends, there is evidence for finer-scale variability throughout the Holocene. The high-resolution XRF data (~25 years) indicate up to four additional periods—each lasting 300–500 years—consisting of increased mineral input from ~6,500–6,100, 5,300–5,000, 3,300–2,800, and 400–0 BP (Fig. 4). These periods correspond with low input of organic matter and detrital carbonate, high bulk density, fine grain size and low sand fraction, and high inputs of base cations, especially K^+ and Mg^{2+}.

The XRF data provide additional information about external versus internal inputs of elements (Fig. 5). Other elements were normalized against Ti to examine silicate mineral composition by removing the variability caused by carbonate and organic-matter dilution. With the exception of Si between 2,500 and 1,500 BP, the ratios of K:Ti, Ca:Ti, and Si:Ti remained fairly stable throughout the Holocene, indicating that detrital inputs were the dominant source of these elements throughout this period (Boës et al. 2011; Kylander et al. 2011). Sr:Ti, P:Ti, and S:Ti were elevated from 6,500 to 3,000 BP (and after 1,200 BP for P and S), suggesting authigenic sources were increasingly important. The ratios of Fe:Ti and Mn:Ti were conservative from 8,700 to 7,400 BP and from ~6,500 to 2,800 BP, reflecting likely detrital sources (Kylander et al. 2011). However, substantial deviations from 7,300 to 6,500 BP and 1,500–500 BP indicate possible altered sediment redox conditions (Kylander et al. 2011) (see Sect. "Discussion").

Vegetation and fire changes

The post-glacial terrestrial plant community (8,200–7,000 BP) was characterized by shrub tundra, dominated by *Alnus* (20–40 %), *Betula* (20–40 %), *Salix* (2–6 %), *Artemesia* (2–4 %), chenopods (1–2 %), and *Cyperaceae* (2–4 %) with sparse forest cover (<50 %) but increasing abundance of *Picea mariana* from ~10 to 40 % (Fig. 6a, b). Low charcoal

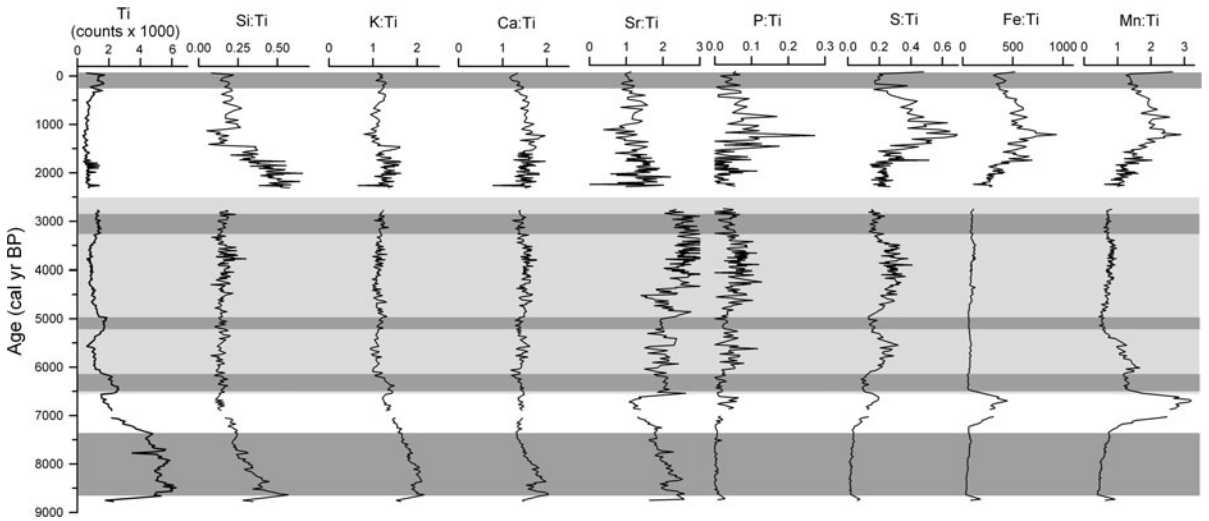

Fig. 5 XRF-derived mineral properties during the Holocene. *Shading* is the same as described in Fig. 4

abundance indicates that fire severity was low during this period (Fig. 6b). During 7,000–2,500 BP, the shrub tundra community changed to a forest-shrub woodland dominated by *P. mariana* (30–40 %) and, increasingly, *Pinus* spp. (10–30 %) (Fig. 6). Fire severity increased more than fourfold during this period (Fig. 6b), associated with the rise in *Pinus* (Fig. 6a). *Alnus* remained an important component of the shrub layer (30–40 %), but *Betula* and *Salix* declined. At ~2,500 BP, the terrestrial plant community shifted once more, with *Alnus* declining to ~20 % and concurrent increases in Poaceae and Cyperaceae (Fig. 6a). Fire severity declined slowly during this period to levels observed during the early Holocene (Fig. 6b).

The aquatic plant and pteridophyte and bryophyte communities show concurrent community change (Fig. 7). *Isoetes* increased in abundance between 6,500 and 2,500 BP, suggesting higher lake levels (Fig. 7a). After 2,500 BP ferns and *Sphagnum* peat mosses increased more than five-fold (Fig. 7b). The increase in *Sphagnum* spores coincides with the initiation of peatlands at three of the five peat sampling locations, and with a decrease in fire across the landscape (Fig. 7b).

Changes in the diatom community

Changes in the diatom community occurred at intervals roughly similar to plant communities (Fig. 8). The

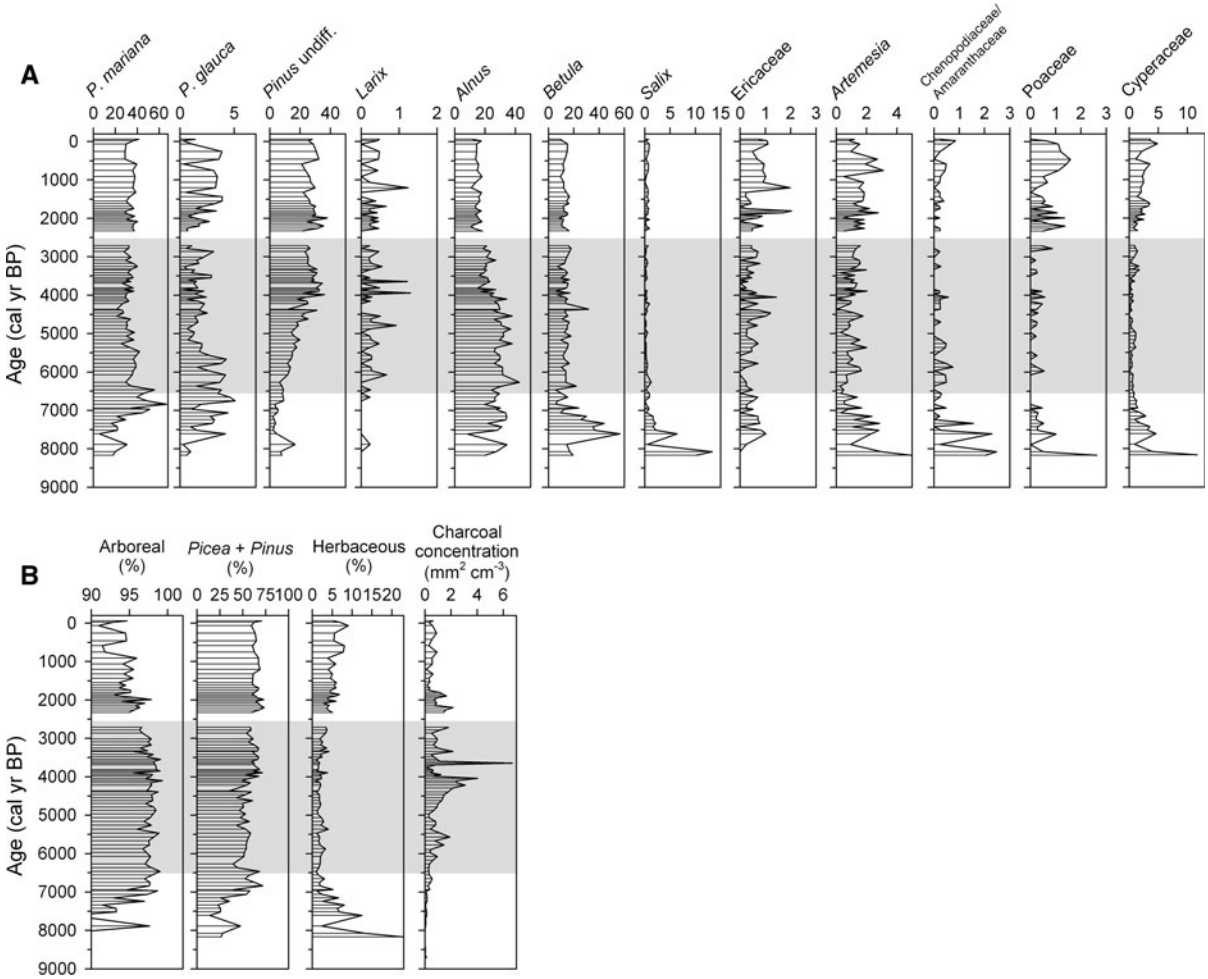

Fig. 6 Terrestrial pollen and fire changes during the Holocene. **a** Pollen percentages for individual taxa. **b** Summary categories for arboreal, forest, herbaceous taxa, pollen concentration in relation to fire severity as recorded by charcoal. The x-axis of each plot is scaled to show changes in each taxon over time. *Light-gray shading* is the same as described in Fig. 4

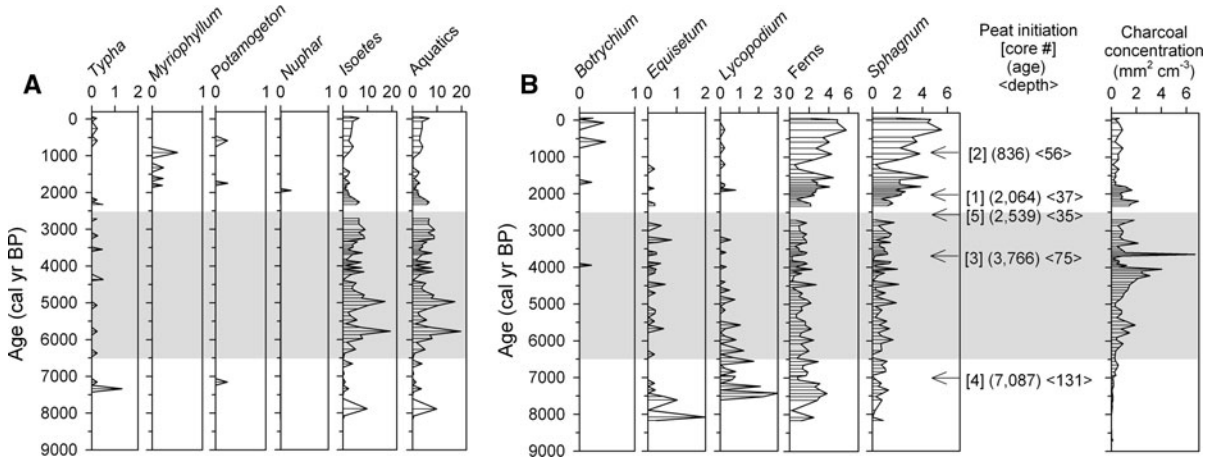

Fig. 7 Changes in **a** aquatic pollen and **b** spores during the Holocene in relation to peat initiation and fire. The x-axis of each plot is scaled to show changes in each taxon over time. *Light-gray shading* is the same as described in Fig. 4

postglacial community (8,500–6,500 BP) was dominated by small, colonial benthic species, *Staurosira construens* and *Staurosirella pinnata* (20–60 %). During the mid-Holocene (~6,500–2,500 BP), the diatom community shifted to acidophilic tychoplanktonic species, including *Aulacoseira* spp. (10–30 %) and *Fragilaria exigua* (~10 %). Epiphytic and epipelic taxa became more abundant (e.g., *Cymbella schubartoides* (5–10 %) and *Pinnularia interrupta* (5–20 %)), suggesting increased shallow-water habitat, although not necessarily lower water tables (see Sect. "Discussion"). During the late Holocene, the planktonic *Cyclotella ocellata* was present at sub-dominant abundance, and *Staurosira construens* and *Staurosirella pinnata* increased to near post-glacial abundance. Planktonic diatoms generally increased during the mid-Holocene and again during the period 1,000–500 BP. DCA axis 1 and cluster analysis indicate substantial community changes at ~6,200 and 2,500 BP, whereas the intervening period corresponds to the dominance of acidophilic taxa (Fig. 8). Diatom-inferred pH declined from ~7 to 5 during the transition from the postglacial period to the mid-Holocene but then rose to pH 5.6–6.3 over the past 2,500 years.

Macronutrients and geochemistry

Geochemical changes responded strongly to the three periods described previously for other proxies: postglacial (9,000–6,500 BP), mid-Holocene (6,500–2,500 BP), and late Holocene (2,500 BP to present) (Fig. 9). During the early postglacial period (9,000–7,500 BP), BSi, TC, TN, TP, and Fe were relatively low, reflecting the oligotrophic status of the lake and the low combined inputs of diatom productivity and terrestrial organic matter. Low BSi:TP and TN:TP ratios suggest Si and N limitation. TC:TN ratios as high as 40 suggest a higher fraction of terrestrial organic inputs, despite the low organic-matter deposition (Fig. 4). $\delta^{13}C$ was −26 to −25‰. $\delta^{15}N$ was more variable but increased steady from 1 to 4‰. The subsequent 1,000 year span of the postglacial/early Holocene period showed significant change (Fig. 9). BSi, TC, and TN rose and then leveled off, but TP and Fe exhibited the largest increase of the Holocene. Substantially elevated Fe:Ti and Mn:Ti ratios, which depart from the overall trend in Ti (Fig. 5), indicate authigenic processing of these elements and suggest that some event affected sediment redox potential (Kylander et al. 2011), such as oxygenation that caused Fe and P to precipitate (Carnigan and Flett 1981). This episode corresponded to a decline in TC:TN from ~40 to 12–14, suggesting a slight increase in algal contributions. While $\delta^{13}C$ remained relatively constant (~−26‰), $\delta^{15}N$ declined to 1–2. Magnetic data indicate that this period occurred during a transition from the deposition of multi-domain ferromagnetic materials (high IRM) to fine-grained, single-domain ferromagnetic materials (high ARM:IRM).

The transition into the mid-Holocene (~6,500–2,500 BP) as characterized by further substantial geochemical changes (Fig. 9). BSi, TC, and TN increased to peak or near-peak levels for the

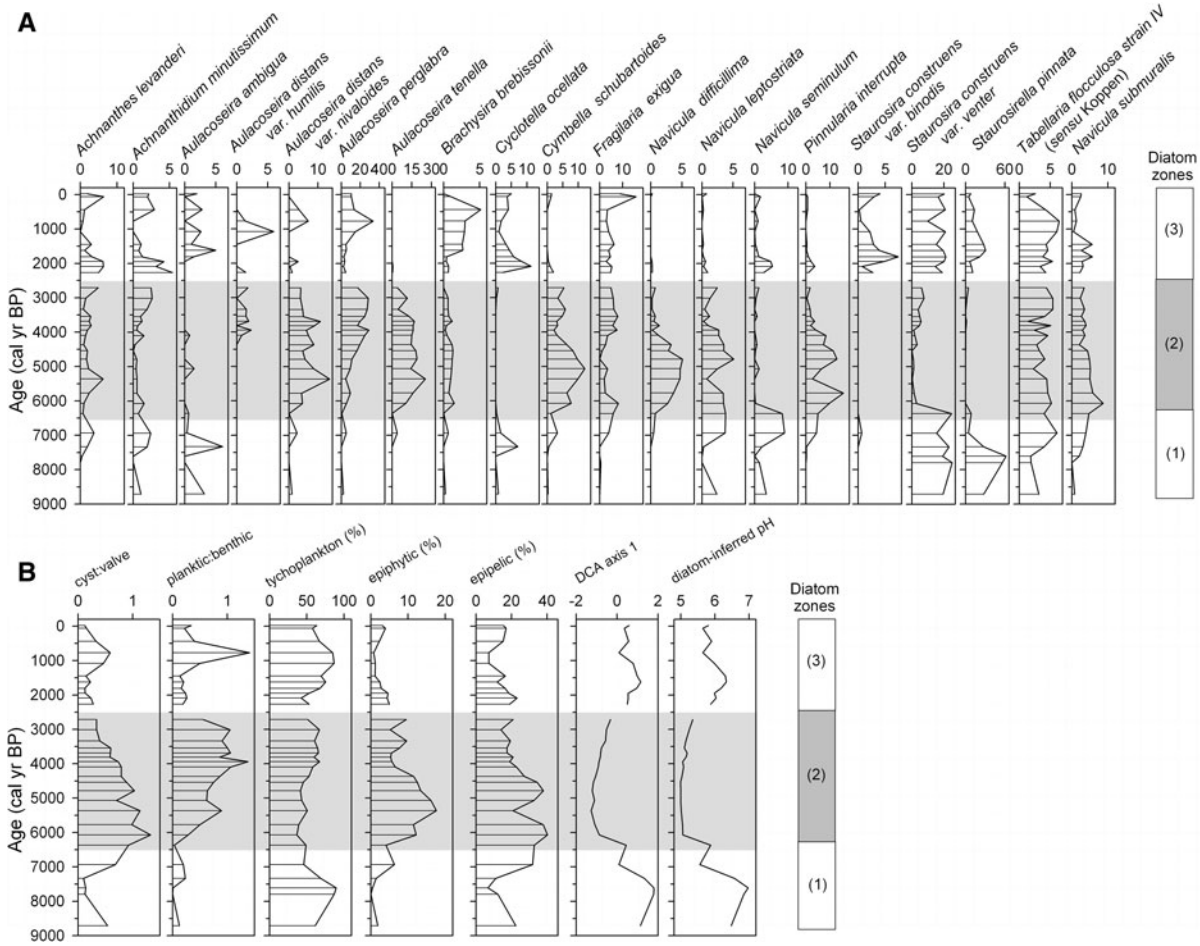

Fig. 8 **a** Diatom species assemblages, and **b** functional groups in Unit Lake during the Holocene. The ratio of planktonic:benthic species treats *Aulacoseira* spp., cyclotelloid species, and planktonic araphids as the planktonic species. Summary analyses include DCA axis 1 scores (SD units) and diatom-inferred pH. The x-axis of each plot is scaled to show changes in each taxon over time. *Shading* is the same as described in Fig. 4

Holocene, but all declined from ~6,500–6,100, 5,300–5,000, and 3,300–2,800 BP at the same time that Ti and other proxies suggest increased allochthonous mineral inputs (Fig. 4). Both TP and Fe declined and then remained stable. BSi:TP and TN:TP rose substantially, suggesting a shift towards greater P limitation and possible terrestrial inputs of N from abundant *Alnus* (Fig. 6). TC:TN fluctuated between 14 and 15, indicating mixed organic contributions from aquatic and terrestrially derived sources. δ^{13}C shifted substantially to ~−29‰, while δ^{15}N rose steadily from 1 to 4‰. Relatively stable and low Fe:Ti and Mn:Ti suggest the predominance of detrital sources for these elements, and the combination of low IRM and high ARM:IRM indicates possible bacterial processing of ferromagnetic minerals to increasingly smaller sizes.

The late Holocene (2,500 BP—present) marked another major shift in geochemical proxies (Fig. 8). BSi peaked around 2,400 BP but declined sharply after 2,000 BP. After the decline around 3,000 BP, TC and TN peaked between 1,500 and 500 BP. TP continued the slow, steady decline, but Fe increased almost sixfold, peaking—as with TC and TN—between 1,500 and 500 BP. The overall decline in BSi caused the BSi:TP ratio to decrease beginning at 2,500 BP, but TN:TP spiked over 40 during the same period, with elevated TC, TN, and Fe. δ^{13}C shifted back to early Holocene levels (~−26‰), whereas δ^{15}N slowly declined from 4 to 3‰. Magnetics data record an

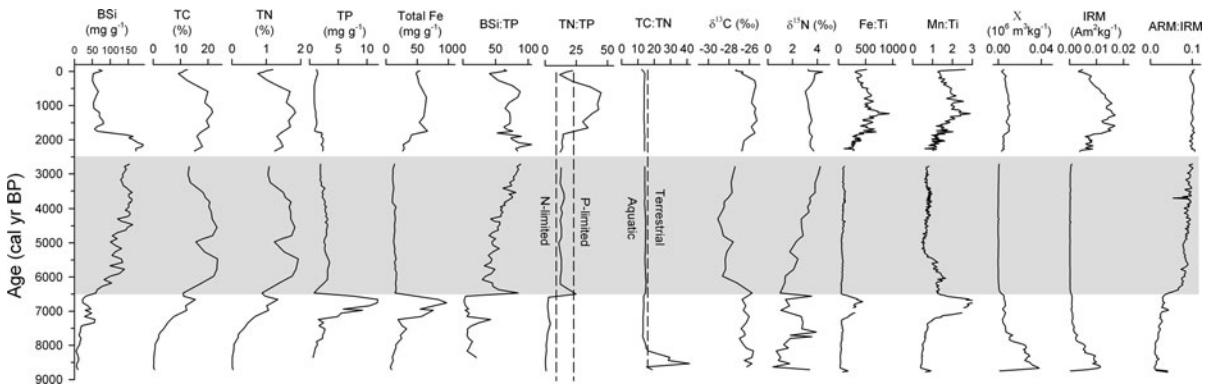

Fig. 9 Geochemical and macronutrient changes during the Holocene. For TN:TP, the *vertical dashed lines* represent approximate sediment TN:TP ratios representing planktonic primary production N limitation (23:1) and P limitation (9:1) (adapted from Kosten et al. 2009). For TC:TN, the 16:1 represents an approximate boundary between aquatic and terrestrial derived organic sources (adapted from Meyers 2003). *Light-gray shading* is the same as described in Fig. 4

increase in IRM, and the XRF data indicate possible redox changes between 1,500 and 500 BP due to elevated Fe:Ti and Mn:Ti ratios.

Although the sediment sampling resolution makes it difficult to describe in detail changes in the surface sediments, the geochemical and macronutrient proxies indicate possible climatic transitions over the past 400 years (Fig. 9). Between 500 and 50 BP, BSi, TC, TN, $\delta^{13}C$, Fe:Ti, and Mn:Ti declined. This was followed by a twentieth-century rise in BSi, TC, TN, BSi:TP, TN:TP, Fe:Ti, and Mn:Ti (Fig. 9).

Discussion

The multi-proxy record from Unit Lake suggests that the timing and magnitude of climate change corresponding to postglacial conditions, HTM, NGC, MCA, LIA, and modern warming can be discerned in the low-Arctic region of western Hudson Bay. We find evidence for a cool and dry postglacial period from 9,000 to 6,500 BP, a warm and moist period from 6,500 to 2,500 BP, and a cool and moist period from 2,500 BP-present. The climatic transitions are coherent across proxies, and both aquatic and terrestrial systems appear to have responded to shifts in temperature and moisture (Fig. 10).

Early postglacial period (9,000–6,500 BP)

The postglacial period was characterized by cooler and possibly drier conditions than present (Fig. 10). The terrestrial ecosystem was dominated by shrub-tundra vegetation (Fig. 6). A relatively open landscape would have provided substantial mineral material to the lake through colluvial and alluvial transport of fine sediments (Figs. 4, 5; Kylander et al. 2011). The aquatic ecosystem was likely confined to the deeper southern basin and was characterized by silty, turbid oligotrophic conditions that constrained aquatic productivity and limited the diatom community to a few generalist taxa common in postglacial environments (*Staurosira construens* and *Staurosirella pinnata*; Haworth 1976) (Figs. 4, 8, 9). Increasing $\delta^{15}N$ from 8,500 to 7,500 BP could have resulted from increased N inputs from *Alnus* (Fig. 6) and the attendant increase in the magnitude of the N cycle (Hu et al. 2001).

Between 7,500 and 6,500 BP, both the terrestrial and aquatic proxies indicate warmer conditions (Fig. 10). The development of a *Picea* woodland indicates the northward migration of the treeline (Fig. 6) that stabilized the landscape and reduced minerogenic inputs, which allowed the diatom community to diversify (Fig. 8). These changes are accompanied by a rise in organic-matter content (Fig. 4), and TC and TN (Fig. 9), with TC:TN ratios suggesting a mix of aquatic and terrestrial organic sources. The sharp rise of Fe:Ti, and Mn:Ti and the subsequent increase in TP and Fe precipitation suggests that the sediment surface became oxygenated (Carnigan and Flett 1981). Increased Fe concentrations are not reflected in χ or IRM but are evident in hysteresis-loop derived high-field susceptibility (data

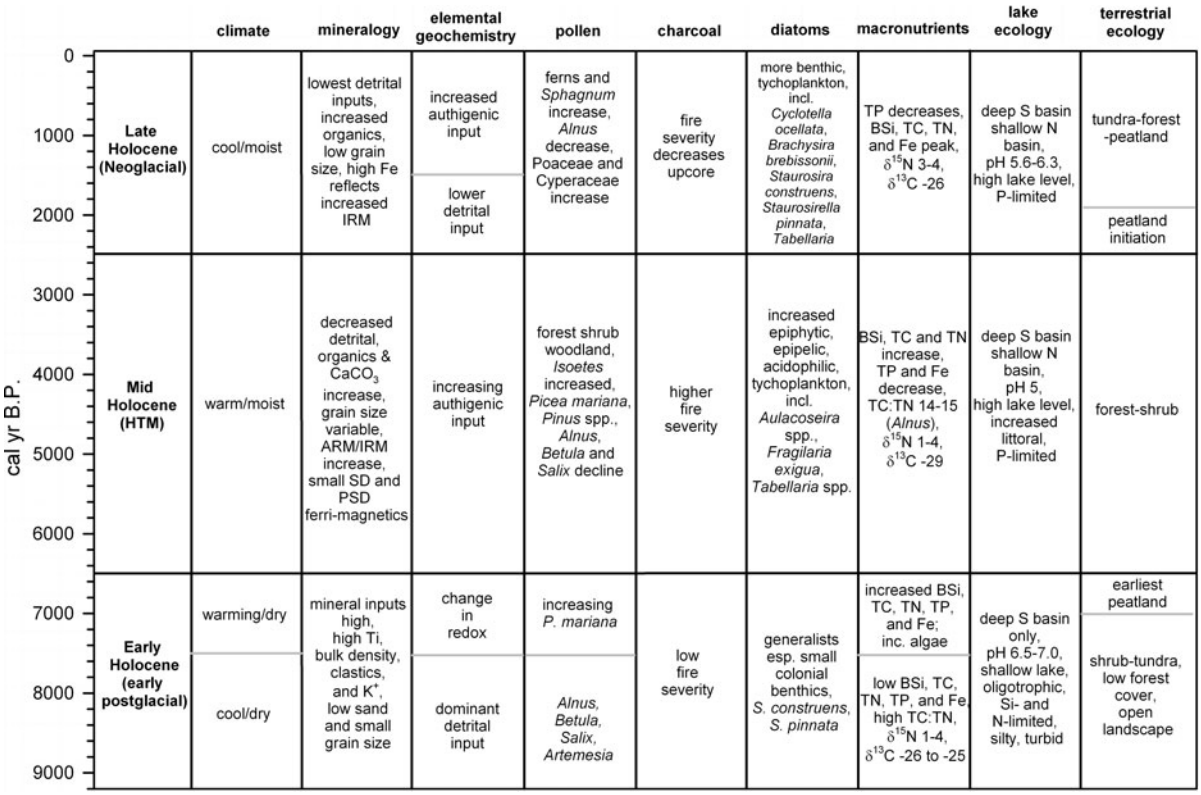

Fig. 10 Paleoecological interpretation and summary of multi-proxy data from Unit Lake core. Major climatic transitions are delineated by *horizontal black lines*. Subdivisions within these periods are denoted by *horizontal gray lines*

not shown), which is consistent with the accumulation of weakly paramagnetic iron-phosphate minerals (Frederichs et al. 2003). Decreasing δ^{15}N values could signal reduced denitrification as sediments became more aerobic (Fig. 9). A possible climatic interpretation is that windier conditions and possibly more pronounced seasonal shifts in temperature increased lake mixing and increased the redox potential of sediments.

This period from 7,500 to 6,500 BP may have also corresponded to increased moisture, as evidenced by the initiation of the oldest peatland bordering the lake (Figs 1, 7, 10), the rise of *P. mariana*, and the dominance of *Alnus* spp.—a genus associated with relatively warm and wet conditions (Moser and MacDonald 1990; Paul et al. 2010).

Holocene thermal maximum (6,500–2,500 BP)

The proxy data indicate that the mid-Holocene, from approximately 6,500–2,500 BP, was relatively warm and wet, constituting the local HTM (Fig. 10). Ti and base cations declined substantially (Fig. 4), suggesting decreased erosion as the landscape became more densely forested, but possibly with increased removal of mineral materials from fringing peatlands (Fig. 6a, b). Arboreal taxa reached their peak of the entire Holocene at this time (Fig. 6a, b). Organic matter, TC, TN, BSi, and $CaCO_3$ all increased during this period (Figs. 4, 9), indicating increased algal productivity (Fortin and Gajewski 2009), although the TC:TN ratio suggests that the organic sources were likely a mix of allochthonous and autochthonous sources (Fig. 9, Meyers 2003). The shift to more-depleted C isotopes (−29 ‰, Fig. 9) could represent increased C inputs from terrestrial vegetation or peat (Kling et al. 1992), or algal productivity derived from isotopically light DIC sources (Kling et al. 1992; Meyers 2003). Although the δ^{13}C trend during the mid-Holocene is distinct and striking, the general range of Holocene δ^{13}C variation (−29 to −25‰) makes it difficult to distinguish algal versus terrestrial organic sources (Meyers 2003).

The beginning of the HTM represents the most significant change (as defined by constrained clustering analysis) in the diatom assemblages. A shift to acidophilic taxa during this time is reflected by the diatom-inferred pH (Fig. 8). Possible mechanisms for the decrease in pH during the HTM include: (1) the development of forest cover dominated by *Picea* spp. (Fig. 6) and the initiation of peatlands (Fig. 6), which contribute humic acids and DOC to the lake, and (2) the subsequent low and decreasing inputs of base cations (Fig. 4) reducing alkalinity (Anderson et al. 2008; Paul et al. 2010). The decrease in pH during the HTM has been documented previously for Arctic lakes (Joynt and Wolfe 2001; Michelutti et al. 2006) and the eastern Canadian sub-Arctic (Fallu et al. 2000). The pH decrease in the Arctic has been ascribed to climate-driven changes in ice cover, which govern dissolved inorganic C speciation through photosynthetic activity (Wolfe 2002). However, in the sub-Arctic the role of terrestrial vegetation, peatlands, and allocthonous organic inputs are likely more important (Fallu et al. 2000).

Several lines of evidence suggest that regional moisture increased at this time. The increase in planktonic diatom taxa (Fig. 8) and *Isoetes* (Fig. 7) suggest higher lake levels than the previous period, although planktonic diatoms might also have increased as peatlands were formed, DOC export increased, and the water column darkened. *Alnus* spp. dominated from 7,000 to 4,000 BP (Fig. 6a). The morphometry of the basin would result in a greatly enlarged littoral zone on the north end as water level rose (Fig. 1c), providing habitat for *Isoetes*, enhanced shoreline for *Alnus*, and greater littoral habitat for benthic, epipelic, and tychoplanktonic forms of diatoms. Detrital sediments tend to be coarser grained (Fig. 4), which is consistent with a higher-energy environment and increased precipitation (Kylander et al. 2011). Increased fire severity at this site might represent greater fuel loading associated with warm, wet conditions (Camill et al. 2003). However, this interpretation is confounded by the correlation between charcoal and *Pinus* sp. (Fig. 6a), which suggests that the arrival of *P. banksiana* could have also increased fire.

Neoglacial period (2,500 BP—present)

The last 2,500 years were a complex climatic period marked by evidence of cool and wet conditions, but with substantial climatic variability at millennial and sub-millennial scales (Fig. 10). Erosion of detrital mineral materials (Ti, base cations) was at the lowest level at any point during the Holocene (Figs. 4, 5), possibly as a result of increased lowland vegetation cover and the expansion of peatlands that could trap erosional inputs. Vegetation changes indicate increasing abundance of *Sphagnum* peat mosses and sedges (Fig. 7b), and are consistent with the evidence of peatland initiation at several locations at <50 cm depth after 3,700 BP (Fig. 7b). Fire severity gradually declined to levels similar to that of the early Holocene (Fig. 6b). The diatom community changed significantly, most notably to higher benthic and tychoplanktonic abundances, in particular small fragilarioids (Fig. 8). Both the diatom changes and peat initiation may have been caused by rising lake levels further enlarging the shallow bench in the north half of the lake where the cored peatlands reside (Fig. 1c). The diatom-inferred pH increases during the late-Holocene and is driven largely by the dominance of the small fragilarioids, which would respond to an increase in the alkalinity of the lake (Rühland et al. 2003) or the expansion of shallow littoral habitat. We observed no relationship between modern-day DOC and pH in a survey of 40 lakes in the region (unpublished data); instead pH is correlated most highly with water column Ca^{2+}, implying that base cations may have a greater influence. While base cations do not change significantly during this time, in contrast to the postglacial period when the higher pH coincided with elevated base cations, an inundation of the landscape may have led to further leaching and weathering of cations (Fig. 4). Increases in *Aulacoseira ambigua, Cyclotella ocellata,* and *Brachysira brebisonii* during the late Holocene strongly influence the modeled increase in pH (Fig. 8). In addition, the habitat preference and wide pH tolerance of *Staurosira* spp. and *Staurosirella pinnata* may have slightly increased the modeled diatom-inferred pH.

Millennial- and sub-millennial-scale climatic features are also evident over the past 2,500 years. One of the most notable events during this period was an apparent warming from 1,500 to 500 BP, possibly associated with the MCA. The rise in organic-matter content, TC, and TN (Figs. 4, 9) suggest increases in terrestrial and algal productivity. However, BSi appears to become uncoupled from organic matter, TC, and TN between 2,000 and 1,500 BP, suggesting

either (1) a switch to a non-diatomaceous plankton community, from Si limitation or habitat shift, or (2) organic inputs primarily derived from terrestrial sources. Moreover, $\delta^{13}C$ and TC:TN remains constant during this period, suggesting no clear trend toward aquatic sources. P deposition was low from 1,500 to 500 BP, suggesting a declining supply of mineral-bound P. χ and IRM increased, consistent with the precipitation of para- and ferrimagnetic iron-oxide phases. There is also an increase in *Aulacoseira* spp. and chrysophyte cysts around 1,000–500 BP, suggesting a longer open-water period (Rühland et al. 2008), stronger seasonality during the MCA, and possibly stronger and warmer summer winds. This indirect evidence of warming is consistent with previous work in central Canada using direct reconstruction of temperature and moisture (MacDonald et al. 2009). Viau and Gajewski (2009) used pollen assemblages to suggest that July and January temperatures and moisture were elevated during this interval. Following this putative warm period, conditions at Unit Lake appear to have become cooler and drier with the onset of the LIA ($\sim$400–50 BP). We observed an increase in Ti, clastics, base cations, and bulk density (suggesting greater aridity and erosion), and a decrease in organic matter, TC, and TN (suggesting lower productivity) (Figs. 4, 9). These LIA-like conditions appear to have occurred periodically throughout the Holocene at $\sim$6,500–6,100, 5,300–5,000, 3,300–2,800, and 400–0 BP (Figs. 4, 5, 9). The rise of Fe:Ti and Mn:Ti from 1,500 to 500 BP, and subsequent decline from 400 BP-present may link sediment redox dynamics to climatic changes as described previously for the early Holocene (8,000–6,500 BP). During these transition periods into and out of the HTM, Unit Lake may have experienced enhanced mixing, causing surface sediments to become more oxidized and leading to increased preservation of Fe and a decrease in $\delta^{15}N$ values (Figs. 4, 9).

Conclusion

The sediment of Unit Lake appears to record broad-scale climate changes, including the transitions from the cool and dry postglacial period (9,000–6,500 BP) to the warm and moist HTM (6,500–2,500 BP) to the cool and moist Neoglacial period (2,500 BP—present). Both terrestrial and aquatic proxies are sensitive to the direct and indirect influences of climate (Fig. 10). Shifts in the plant community, changes in fire severity (a response to productivity/fuel loading), and peatland initiation indicate that the terrestrial system was likely responsive to both regional temperature and effective moisture. The aquatic system responded to apparent changes in lake level, temperature, and nutrients based on changes in diatom communities, macronutrients, pollen, and inferred water chemistry and lake ecology. Further high-resolution analysis of the physical and biological properties of the sediment (e.g., chironomid-based temperature reconstructions) could offer a more direct reconstruction of specific climate variables in this region. Finer-scale changes are also evident at sub-millennial scales, such as the MCA, LIA, and twentieth-century warming. High-resolution geochemical data suggest 300- to 500-year-long dry periods at $\sim$6,500–6,100, 5,300–5,000, 3,300–2,800, and 400–0 BP. Our results are in broad agreement with previous assessments of Holocene climatic change in central Canada, which generally suggest cool and dry conditions 10,000–6,000 BP, warmer and wetter conditions between 8,000 and 3,000 BP, and cooler, moist conditions from 3,500 BP—present (Huang et al. 2004; Kaufman et al. 2004; Viau and Gajewski 2009; Adams and Finkelstein 2010; Paul et al. 2010; Peros et al. 2010; Tillman et al. 2010). These results suggest that terrestrial and aquatic ecosystem dynamics in the western Hudson Bay region are sensitive to past climate change and are likely to change substantially with future changes in temperature and precipitation. Analysis of additional lake sediment records in this region will be valuable for determining the extent to which these climatic transitions are coherent across a heterogeneous landscape.

Acknowledgments Thanks to Tom Brown for assistance with radiocarbon dating and Dan Engstrom for help with ^{210}Pb dating. Thanks also to Jon Kovac for assistance in the field. We thank Darrell Kaufman and two anonymous reviewers for helpful comments on earlier versions of this manuscript. This study was supported by National Science Foundation grants DEB-0743364, DEB-0904050, DEB 0092704, and DBI-0520803. The IRM was made possible through the Instrumentation and Facilities program of the National Science Foundation, Earth Science Division and by funding from the University of Minnesota. Initial core processing was performed at the Limnological Research Center (University of Minnesota). Any opinions, findings, and conclusions or recommendations expressed are those of the authors and do not necessarily reflect the views of the NSF. This work was also

funded, in part, by a grant to St Olaf from the Howard Hughes Medical Institution.

References

Adams JK, Finkelstein S (2010) Watershed-scale reconstruction of middle and late Holocene paleoenvironmental changes on Melville Peninsula, Nunavut, Canada. Quat Sci Rev 29:2302–2314

Adrian R, O'Reilly CM, Zagarese H, Baines SB, Hessen DO, Keller W, Livingstone DM, Sommaruga R, Straile D, Van Donk E, Weyhenmeyer GA, Winder M (2009) Lakes as sentinels of climate change. Limnol Oceanogr 54: 2283–2297

Anderson NJ, Brodersen KP, Ryves DB, McGowan S, Johansson LS, Jeppesen E, Leng MJ (2008) Climate versus in-lake processes as controls on the development of community structure in a low-arctic lake (South-West Greenland). Ecosystems 11:307–324

Appleby PG, Oldfield F (1978) The calculation of lead-210 dates assuming a constant rate of supply of unsupported ^{210}Pb to the sediment. Catena 5:1–8

Bennett KD (1996) Determination of the number of zones in a biostratigraphical sequence. New Phytol 132:155–170

Blaauw M (2010) Methods and code for 'classical' age-modelling of radiocarbon sequences. Quat Geochron 5: 512–518

Boës X, Rydberg J, Martinez-Cortizas A, Bindler R, Renberg I (2011) Evaluation of conservative lithogenic elements (Ti, Zr, Al, and Rb) to study anthropogenic element enrichments in lake sediments. J Paleolimnol 46:75–87

Camburn KE, Charles DF (2000) Diatoms of low-alkalinity lakes in the northeastern United States. The Academy of Natural Sciences of Philadelphia Special Publication 18. p 152

Camill P, Umbanhowar CE, Teed R, Geiss CE, Aldinger J, Dvorak L, Kenning J, Limmer J, Walkup K (2003) Late-glacial and Holocene climatic effects on fire and vegetation dynamics at the prairie-forest ecotone in south-central Minnesota. J Ecol 91:822–836

Carnigan R, Flett RJ (1981) Postdepositional mobility of phosphorus in lake sediments. Limnol Oceanogr 26: 361–366

Clark JS, Hussey T, Royall PD (1996) Presettlement analogs for quaternary fire regimes in eastern North America. J Paleolimnol 16:79–96

Conley DJ (1998) An interlaboratory comparison for the measurement of biogenic silica in sediments. Mar Chem 63: 39–48

Conley DJ, Schelske CL (1993) Potential role of sponge spicules in influencing the silicon biogeochemistry of Florida lakes. Can J Fish Aquat Sci 50:296–302

Dean WE Jr (1974) Determination of carbonate and organic matter in calcareous sediments and sedimentary rocks by loss-on-ignition: comparison with other methods. J Sediment Petrol 44:271–272

Engstrom DR, Fritz SC (2006) Coupling between primary terrestrial succession and the trophic development of lakes at Glacier Bay, Alaska. J Paleolimnol 35:873–880

Engstrom DR, Wright Jr HR (1984) Chemical stratigraphy of lake sediments as a record of environmental change. In: Haworth EY, Lund JWG (eds) Lake sediments and environmental history. University of Minnesota Press, Minneapolis, pp 11–67

Fægri K, Iversen J, Kaland PE, Kryzywinski K (1989) Textbook of pollen analysis, 4th edn. Wiley, New York

Fallu MA, Allaire N, Pienitz R (2000) Freshwater diatoms from northern Québec and Labrador (Canada): species–environment relationships in lakes of boreal forest, forest-tundra and tundra regions. Bibl Diatom Band 45. E. Schweizerbart, Germany, p 200

Fortin MC, Gajewski K (2009) Assessing the use of sediment organic, carbonate and biogenic silica content as indicators of environmental conditions in Arctic lakes. Polar Biol 32:985–998

Frederichs T, von Dobeneck T, Bleil U, Dekkers MJ (2003) Towards the identification of siderite, rhodochrosite, and vivianite in sediments by their low-temperature magnetic properties. Phys Chem Earth 28:669–679

Fritz SC, Cumming BF, Gasse F, Laird K (1999) Diatoms as indicators of hydrologic and climatic change in saline lakes. In: Stoermer EF, Smol JP (eds) The diatoms: applications for the environmental and earth sciences. Cambridge University Press, Cambridge, pp 41–72

Geiss CE, Umbanhowar CE, Camill P, Banerjee SK (2003) Sediment magnetic properties reveal Holocene climate change along the Minnesota prairie-forest ecotone. J Paleolimnol 30:151–166

Grimm EC (1987) CONISS, a Fortran 77 program for stratigraphically constrained cluster analysis by the method of incremental sum of squares. Comput Geosci 13:13–35

Hansen BCS, Engstrom DR (1985) A comparison of numerical and qualitative methods of separating pollen of black and white spruce. Can J Bot 63:2159–2163

Haworth EY (1976) Two late-glacial (late Devensian) diatom assemblage profiles from northern Scotland. New Phytol 77:227–256

Hill MO, Gauch HG (1980) Detrended correspondence-analysis—an improved ordination technique. Vegetatio 42: 47–58

Hoenicke R, Stapanian MA, Arent LJ, Metcalf RC (1991) Consequences of pH measurement errors. Freshw Biol 25(2):261–278

Hu FS, Finney BP, Brubaker LB (2001) Effects of Holocene *Alnus* expansion on aquatic productivity, nitrogen cycling, and soil development in southwestern Alaska. Ecosystems 4:358–368

Huang CC, MacDonald G, Cwynar L (2004) Holocene landscape development and climatic change in the low Arctic, Northwest Territories, Canada. Palaeogeogr Palaeoclimatol Palaeoecol 205:221–234

IPCC (2007) Climate Change 2007: Synthesis Report. Contribution of Working Groups I, II and III to the Fourth Assessment Report of the Intergovernmental Panel on Climate Change [Core Writing Team, Pachauri RK, Reisinger A (eds)]. IPCC, Geneva, p 104

Joynt EH, Wolfe AP (2001) Paleoenvironmental inference models from sediment diatom assemblages in Baffin Island lakes (Nunavut, Canada) and reconstruction of summer water temperature. Can J Fish Aquat Sci 58:1222–1243

Juggins S (2003) C2 Software for ecological and palaeoecological data analysis and visualisation User Guide Version 1.3. University of Newcastle

Kaufman DS, Ager TA, Anderson NJ, Anderson PM, Andrews JT, Bartlein PJ, Brubaker LB, Coats LL, Cwynar LC, Duvall ML, Dyke AS, Edwards ME, Eisner WR, Gajewski K, Geirsdóttir A, Hu FS, Jennings AE, Kaplan MR, Kerwin MW, Lozhkin AV, MacDonald GM, Miller GH, Mock CJ, Oswald WW, Otto-Bliesner BL, Porinchu DF, Rühland K, Smol JP, Steig EJ, Wolfe BB (2004) Holocene thermal maximum in the western arctic (0–180°W). Quat Sci Rev 23:529–560

Kling GW, Fry B, O'Brien WJ (1992) Stable isotopes and planktonic trophic structure in Arctic lakes. Ecology 73: 561–566

Kosten S, Huszar VLM, Mazzeo N, Scheffer M, Sternberg LDL, Jeppesen E (2009) Lake and watershed characteristics rather than climate influence nutrient limitation in shallow lakes. Ecol Appl 19:1791–1804

Krammer K, Lange-Bertalot H (1986–1991) Bacillariophyceae. 1–4. Teil: Naviculaceae. In: Ettl H, Gärtner G, Gerloff J, Heynig H, Mollenhauer D (eds) Süßwasserflora von Mitteleuropa. Bands 2/1–2/4, Gustav Fischer Verlag, Stuttgart, p 876, p 596, p 576, p 437

Kylander ME, Ampel L, Wohlfarth B, Veres D (2011) High-resolution X-ray fluorescence core scanning analysis of Les Echets (France) sedimentary sequence: new insights from chemical proxies. J Quat Sci 26:109–117

Leavitt PR, Fritz SC, Anderson NJ, Baker PA, Blenckner T, Bunting L, Catalan J, Conley DJ, Hobbs WO, Jeppesen E, Korhola A, McGowan S, Rühland K, Rusak JA, Simpson GL, Solovieva N, Werne J (2009) Paleolimnological evidence of the effects on lakes of energy and mass transfer from climate and humans. Limnol Oceanogr 54:2330–2348

MacDonald GM, Porinchu DF, Nicolas R, Kremenetsky KV, Kaufman DS (2009) Paleolimnological evidence of the response of the central Canadian treeline zone to radiative forcing and hemispheric patterns of temperature change over the past 2000 years. J Paleolimnol 41:129–141

Matile GLD, Keller GR (2006) Surficial geology of the Nejanilini Lake map sheets (NTS 64P), Manitoba, Surficial Geol. Compilation Maps Ser., SG-64P, scale 1:250,000, Manitoba Sci. Technol. Energy and Mines, Manitoba Geol. Surv., Winnipeg, Manitoba, Canada

McAndrews JH, Berti A, Norris G (1973) Key of quaternary pollen and spores of the Great Lake Region. Life Sci. Misc. Publ., R. Ont. Mus.

Meyers P (2003) Applications of organic geochemistry to paleolimnological reconstructions: a summary of examples from the Laurentian Great Lakes. Org Geochem 34: 261–289

Michelutti N, Douglas MSV, Wolfe AP, Smol JP (2006) Heightened sensitivity of a poorly buffered high arctic lake to late-Holocene climatic change. Quat Res 65:421–430

Michelutti N, Wolfe AP, Briner JP, Miller GH (2007) Climatically controlled chemical and biological development in Arctic lakes. J Geophys Res Biogeosci 112(G3). doi: 10.1029/2006JG000396

Moser KA, MacDonald GM (1990) Holocene vegetation change at treeline north of Yellowknife, Northwest Territories, Canada. Quat Res 34:227–239

Moskowitz BM, Frankel RB, Flanders PJ, Blakemore RP, Schwartz BB (1988) Magnetic properties of magnetotactic bacteria. J Magn Magn Mater 73:273–288

Paul CA, Rühland KM, Smol JP (2010) Diatom-inferred climatic and environmental changes over the last similar to 9000 years from a low Arctic (Nunavut, Canada) tundra lake. Palaeogeogr Palaeoclimatol Palaeoecol 291:205–216

Peros M, Gajewski K, Paull T, Ravindra R, Podritske B (2010) Multi-proxy record of postglacial environmental change, south-central Melville Island, Northwest Territories, Canada. Quat Res 73:247–258

Rouse WR (1991) Impact of Hudson Bay on the terrestrial climate of the Hudson Bay Lowlands. Arct Alp Res 23:24–30

Rühland K, Priesnitz A, Smol JP (2003) Paleolimnological evidence from diatoms for recent environmental changes in 50 lakes across Canadian arctic treeline. Arct Antarct Alp Res 35:110–123

Rühland K, Paterson AM, Smol JP (2008) Hemispheric-scale patterns of climate-related shifts in planktonic diatoms from North American and European lakes. Glob Change Biol 14:2740–2754

Schindler DW (2009) Lakes as sentinels and integrators for the effects of climate change on watersheds, airsheds, and landscapes. Limnol Oceanogr 54:2349–2358

Schledewitz DCP, Lindal D (2002) Nejanilini Lake, Bedrock Geology Compilation Map, NTS 64P, scale 1:250,000. Manitoba Sci. Technol. Energy and Mines, Manitoba Geol. Surv., Winnipeg, Manitoba, Canada

Scott PA, Fayle DCF, Bentley CV, Hansell RIC (1988) Large-scale changes in atmospheric circulation interpreted from patterns of tree growth at Churchill, Manitoba, Canada. Arct Alp Res 20:199–211

Stuiver M, Reimer PJ, Reimer R (1999) CALIB radiocarbon calibration (HTML Version 6.0). http://calib.qub.ac.uk/calib/

Tardif JC, Conciatori F, Leavitt SW (2008) Tree rings, delta C-13 and climate in *Picea glauca* growing near Churchill, subarctic Manitoba, Canada. Chem Geol 252:88–101

Tillman PK, Holzkämper S, Kuhry P, Sannel ABK, Loader NJ, Robertson I (2010) Long-term climate variability in continental subarctic Canada: a 6200-year record derived from stable isotopes in peat. Palaeogeogr Palaeoclimatol Palaeoecol 298:235–246

Tivy A, Howell SEL, Alt B (2011) Trends and variability in summer sea ice cover in the Canadian Arctic based on the Canadian Ice Service Digital Archive, 1960–2008 and 1968–2008. J Geophys Res-Oceans 116. doi:10.1029/2009JC005855

Triplett L (2002) Standard operating procedures for grain size analysis sample preparation. Limnological Research Center, Minneapolis

Viau AE, Gajewski K (2009) Reconstructing millennial-scale, regional paleoclimates of boreal Canada during the Holocene. J Clim 22:316–330

Wolfe AP (2002) Climate modulates acidity of Arctic lakes on millennial time scales. Geology 30:215–218

Yu Z, Bielman D, Frolking S, MacDonald G, Roulet N, Camill P, Charman D (2011) Peatlands in the global carbon cycle. EOS 92:97–98